

Laser-driven Ultrafast Dynamics of a Fractional Quantum Hall System

Ammar Kirmani,¹ Benedikt Fauseweh,² and Jian-Xin Zhu^{1,3}

¹*Theoretical Division, Los Alamos National Laboratory, Los Alamos, New Mexico 87545, USA**

²*Department of Physics, TU Dortmund University, 44227 Dortmund, Germany[†]*

³*Center for Integrated Nanotechnologies, Los Alamos National Laboratory, Los Alamos, New Mexico 87545, USA[‡]*

Fractional quantum Hall (FQH) systems are strongly interacting electron systems with topological order. These systems are characterized by novel ground states, fractionally charged and neutral excitations. The neutral excitations are dominated by a low-energy collective magnetoroton mode. Here we derive and use a quasi-one-dimensional model to investigate the ultrafast nonequilibrium dynamics of a laser-driven FQH system within a two-Landau-level approximation. As opposed to the traditional and synthetic bilayers, our model accounts for interactions where electrons can scatter from one Landau-level to another. By performing exact time evolution of the system, we create an out-of-equilibrium state following the laser pulse that shows rich physics. Our calculations show the presence of non-trivial excited modes. One of these modes is electromagnetically active and represent density oscillations of *magnetoplasmon* mode. Another mode is identified by evaluating the overlap of the initial state and the out-of-equilibrium state following the laser pulse with a quadrupole operator. This mode is analogous to the chiral-graviton mode for FQH systems recently measured in experiments [Nature **628**, 78 (2024)]. Our results show that a linearly-polarized pulse field can excite the graviton mode when inter-Landau level scattering occurs.

Introduction.— Fractional quantum Hall (FQH) systems are a prototypical example of strongly correlated physical systems with rich novel phenomena like topological order, quantum geometry and excitations that follow fractional statistics [1, 2]. The neutral excitations of FQH systems are dominated by a collective coherent oscillation mode usually called Girvin-MacDonald-Platzman magnetoroton mode [3, 4]. In the long-wavelength limit $k \rightarrow 0$, the magnetoroton becomes a quadrupole excitation that carries $L = 2$ angular momentum along with the excitation of an underlying quantum geometry metric analogous to the passing of gravitational waves in a medium [1]. Another novel consequence of the presence of quantum geometry and topology in FQH systems is the quantization of Hall viscosity [5–7]. FQH phase is characterized by the quantization of transverse component of resistivity at low temperatures. This is measured in 2D electrons with density ρ in the presence of high perpendicular magnetic field B at fractional filling $\nu = \rho h/eB$ (h being Planck’s constant and e is the electron charge). Among many odd-denominator fractional filling states observed experimentally [8, 9] and theoretically explained [10, 11], the first observed FQH state at $\nu = \frac{1}{3}$ is of particular interest. It was shown that fractional $\frac{1}{3}$ state can host charged excitations like quasi-particle (quasi-hole) of $e/3$ sometimes called *anyons* [2]. It was not until recently that experiments performed on this FQH state gave first direct observation of exchange statistics of fractionally charged particles (anyons) [12]. Furthermore, interest in this state is rekindled due to the observation of two $e/3$ quasi-particles scattering into an electron and “Andreev reflected” quasi-hole [13]. Besides its experimental accessibility, this state has also been readily studied theoretically on different geometries [14–17]. Moreover, a long wavelength low-energy excita-

tion mode of $\frac{1}{3}$ FQH state has been excited in inelastic linearly-polarized light scattering experiments [18]. This mode was identified later on as a chiral-graviton mode that can be excited through circularly polarized light [19]. Another experiment has also excited this mode through two-photon processes in FQH-1/3 state [20]. Despite such experiments, the theoretical understanding of the dynamics of a multi-Landau-level FQH system has been limited.

In this Letter, we present ultra-fast dynamics of the FQH system is driven out-of-equilibrium by a laser pulse field. The system is initially in $\nu = \frac{1}{3}$ FQH state. We show that when all inter-two-level scattering terms are considered, a short time linearly-polarized light with frequency near Landau level gap can excite chiral-graviton mode below magnetoplasmon mode. We note that while optically driven synthetic bilayers have been recently proposed [21, 22] to host new types of FQH states [23, 24], as in conventional semiconductor bilayers [25–28], the electronic systems are assumed to thermalize to the Floquet ground state in the rotating framework of the optical drive field. Therefore, the problem studied in the present work is quite distinct from the situations studied before.

Model Hamiltonian.— We consider a 2D spinless electronic system defined on the surface of torus with lengths L_x and L_y , as shown in Fig. 1 in the presence of both a high perpendicular static magnetic field and a time-dependent electric field from the laser pulse. In the Landau gauge, both magnetic and electric fields can be described by the vector potential $\mathbf{A} = \mathbf{A}_{\text{static}}(\mathbf{r}) + \mathbf{A}_{\text{EM}}(t)$ with $\mathbf{A}_{\text{static}} = (0, Bx, 0)$ and $\mathbf{A}_{\text{EM}} = (0, A_{\text{EM}}(t), 0)$. The single-particle states in this gauge compatible with torus

boundary conditions are given by [29]

$$\phi_{n,j}(\mathbf{r}) = \frac{1}{\sqrt{\mathcal{N}_n}} \sum_k e^{i \frac{(X_j+kL_x)y}{\ell_B^2}} e^{-\frac{(x+X_j+kL_x)^2}{2\ell_B^2}} H_n\left(\frac{x+X_j+kL_x}{\ell_B}\right) \quad (1)$$

Where $X_j = \frac{2\pi j}{L_y} \ell_B^2$ with $\ell_B = \sqrt{\hbar/eB}$ being the magnetic length. $\mathcal{N}_n = L_y \sqrt{\pi} 2^n n! \ell_B$ is the normalization constant and H_n is Hermite polynomial of order n . For each Landau level n , index j runs from $0, 1, \dots, N_\phi - 1$, where $N_\phi = L_x L_y / (2\pi \ell_B^2)$ is the number of flux quanta (Landau orbitals) passing through the system. Within this Landau orbital basis, we are able to write the system Hamiltonian as $\hat{H} = \hat{H}_{sp} + \hat{H}_{int}$, with

$$\hat{H}_{sp} = \omega_c \sum_j \hat{n}_{1,j} + \Gamma_{EM}(t) [\sum_j c_{0,j}^\dagger c_{1,j} + \text{H.c.}], \quad (2)$$

describing the coupling of electrons with the laser pulse field up to the first Landau level (LL1), and

$$\hat{H}_{int} = \sum_{\{n_i, j_i\}} V_{j_1, j_2; j_3, j_4}^{n_1, n_2; n_3, n_4} c_{n_1, j_1}^\dagger c_{n_2, j_2}^\dagger c_{n_3, j_3} c_{n_4, j_4}, \quad (3)$$

describing the Coulomb interaction with $V_{n_1, n_2; n_3, n_4}^{j_1, j_2; j_3, j_4}$ the amplitude of two-particle scattering processes due to the repulsive interactions. Here the operators $c_{m,j}$, $c_{m,j}^\dagger$ ($\hat{n}_{m,j} \equiv c_{m,j}^\dagger c_{m,j}$) destroy or create an electron in m -th Landau level (LL) at j -th orbital localized around $2\pi j \ell_B^2 / L_y$ along the axis of the cylinder. The quantity ω_c is the level-spacing between Landau levels 0-1 (see Fig. 1). In each Landau level, cyclotron frequency of electron is quantized in units of $\omega_c = eB/m^*$ (m^* is electron's effective-mass). The laser field coupling strength $\Gamma_{EM} = \frac{eA_{EM}(t)}{\sqrt{2m^* \ell_B}}$. We also note for electrons interacting through Coulomb repulsion in the system, the Coulomb energy $E_c = e^2/\epsilon \ell_B$ (ϵ being di-electric constant) is also an important energy scale. The interaction part of our Hamiltonian Eq. (3) contains both intra- and inter-level scattering processes. Throughout the work, we use a short pulse form $A_{EM}(t) = A_0 e^{-\frac{(t-t_c)^2}{2t_d^2}} \cos[\omega_0(t-t_c)]$ where t_d is time delay, t_c is the center time for the pulse and ω_0 is the frequency of incoming laser [30].

In the absence of the pulse field and for large positive ω_c , our fermions are in the ground state of the system, containing N electrons, such that the filling factor is $\nu = N/N_\phi = 1/3$. Also the system Hamiltonian commutes with the center of mass-momentum operator $\hat{K} = \sum_{j,n} j c_{n,j}^\dagger c_{n,j}$ (in Landau gauge) and momentum

transfer by the laser pulse is considered to be negligible. Hence, our many-body dynamics is contained in the momentum eigen-sector of the initial state. To include the effects of the out-of-equilibrium physics under the influence of a laser-pulse, the Hamiltonian includes

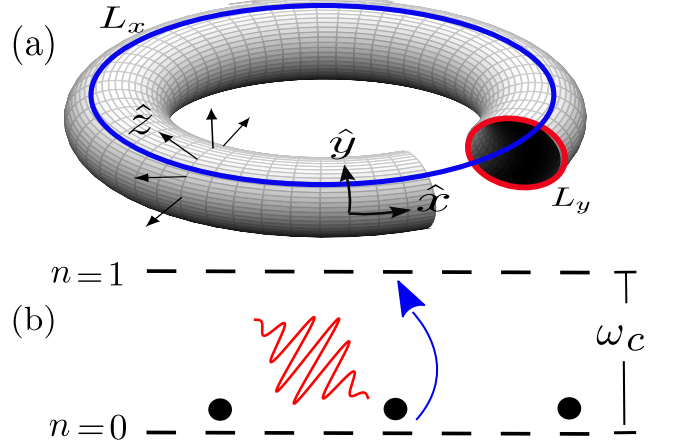


FIG. 1. (a) Torus with lengths L_x and L_y . Magnetic field is pointing along \hat{z} . (b) A schematic of a two-level FQH system. Initially, the system is in fractional $\nu = 1/3$ state occupying the LLL ($n = 0$). This state is then laser-driven creating excitations to the first Landau level ($n = 1$). The energy difference between the two levels is ω_c .

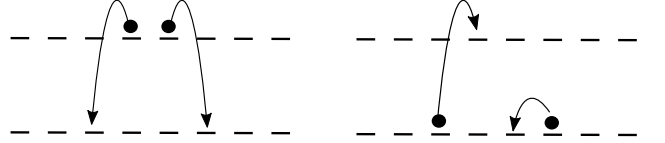


FIG. 2. Two-electron virtual processes that do not conserve Landau level index.

both scattering processes that conserve Landau level index $n_1 + n_2 = n_3 + n_4$ and ones that break the level index i.e. $n_1 + n_2 \neq n_3 + n_4$. The latter is schematically illustrated in Fig. 2. This is the consequence of an electron scattering from one level to another and is ignored in traditional and synthetic bi-layers [21]. We avoid large scale Hilbert space by truncating Hamiltonian to LL1 and by considering low-intensity radiation. This assumption is further validated by another resonant inelastic light experiment for FQH $\frac{1}{3}$ state showing most features related to excitations from LLL to LL1 [18]. Coulomb's interaction potential for torus boundary conditions is $V(\mathbf{r}) = \sum_{s,t} e^2/\epsilon |\mathbf{r} + sL_x \hat{x} + tL_y \hat{y}|$ where \hat{x} , \hat{y} are the units vectors along the two axes of the torus [14]. We obtain the matrix elements

$$V_{j_1, j_2, j_3, j_4}^{n_1, n_2, n_3, n_4} = \frac{\delta'_{j_1+j_2, j_3+j_4}}{2L_x L_y} \sum_{\mathbf{q}, \mathbf{q} \neq 0} \delta_{q_y, t \frac{2\pi}{b}} \delta_{q_x, s \frac{2\pi}{a}} \delta'_{j_1-j_4, t} \frac{2\pi e^2}{\epsilon q} C_{n_1, n_4}(-\mathbf{q}) C_{n_2, n_3}(\mathbf{q}) e^{-i2\pi s \frac{j_1-j_3}{N_\phi}} e^{-\frac{q_x^2 + q_y^2}{2} \ell_B^2} \quad (4)$$

Where $C_{0,0}(\mathbf{q}) = 1$, $C_{1,1}(\mathbf{q}) = 1 - \frac{|q|^2 \ell_B^2}{2}$ and $C_{1,0}(\mathbf{q}) = \frac{q_y + iq_x}{\sqrt{2}} \ell_B = [C_{0,1}(-\mathbf{q})]^*$. Prime over a delta function indicates that it is defined modulo N_ϕ . Fractional $1/3$ state [10] is the ground state of the Hamiltonian $\sum_{j_i} V_{j_1, j_2, j_3, j_4}^{0,0,0,0} c_{j_1}^\dagger c_{j_2}^\dagger c_{j_3} c_{j_4}$ and is adiabatically connected to period-three charge-density $|100, 100, 100, 100, \dots\rangle$ [31, 32] (for short-range potential $\nabla^2 \delta(\mathbf{r})$). The physics of FQH systems are usually studied in the limit of large level-spacing and the Hamiltonian for single Landau level is diagonalized. This is due the assumption that Coulomb interaction is weak to scatter electron from one level to another in the large magnetic field limit which is not always true [33]. We have first verified that the ground state of the system Hamiltonian involving virtual process for various values of level spacing is indeed the fractional- $\frac{1}{3}$ quantum Hall state (See Supplemental Material (SM) [34] for more details).

Dynamical observables. We turn on a laser-pulse on the FQH- $\frac{1}{3}$ state $|\Psi_0\rangle$ at $t = 0$ and let the system evolve through Schrodinger equation as $|\Psi(t)\rangle = \hat{T} e^{-i \int_0^t \hat{H}(t') dt'} |\Psi_0\rangle$, where \hat{T} is the time ordering operator and $\Psi(t)$ is our out-of-equilibrium state. The time-ordering is achieved by discretizing the time-dependent matrix exponential in small time steps. The dynamical response of the system can be understood with time-dependent quantities like mean occupation number of LL1, $\hat{N}_1 = \sum_j \hat{n}_{1,j}$, the fidelity $|\langle \Psi_0 | \Psi(t) \rangle|^2$ and structure factor $\mathcal{S}(\mathbf{q}) = \langle \hat{\rho}_{\mathbf{q}} \hat{\rho}_{-\mathbf{q}} \rangle$ where $\rho_{\mathbf{q}}$ is the projected density (see SM [34]) and current in system

$$\hat{J}_{x/y} = \frac{\hbar(i/1)}{m\sqrt{2}} \sum_j \left(c_{1,j}^\dagger c_{0,j} \mp c_{0,j}^\dagger c_{1,j} \right). \quad (5)$$

The details of this quantity is given in the SM [34].

Results. We consider level-spacing $\omega_c < E_c$, i.e. the level spacing is less than Coulomb energy scale. The ratio of these energies $\kappa \equiv \frac{e^2}{\hbar\omega_c \epsilon \ell_B}$ is magnetic field dependent ranging from $2.6/\sqrt{B[T]}$ for Ga-As to $22.5/\sqrt{B[T]}$ for Al-As justifying the our approximation for fractional $\nu = 1/3$ Hall system usually observed at $B \sim 10$ Tesla [35]. In Fig. 3, we present observables like fidelity, mean-excitation number and spectrum of $d[\hat{J}(t)]/dt$ after the pulse for $\omega_c = E_c/2$ for $L_y = \sqrt{2\pi}18\ell_B$. Fig. 3 (a-b) gives the excitations to LL1 and the fidelity. The current $\hat{J}_{x,y}$ in the Fig. 3 (c-d) remains oscillating with multiple periods after the pulse is finished. Fig. 4 gives the spectrum of current of $\mathcal{J}_y(\omega) = \mathcal{F}_t \left[\frac{d}{dt} \hat{J}_y(t) \right](\omega)$ for $L_y = \sqrt{2\pi}18\ell_B$ (liquid limit) and $L_y = 2\pi\ell_B$ (near-TT limit). There are two modes as seen from the spectrum for low-intensity short time pulses one at ω_c and another blue-shifted from ω_c . The presence of these modes are robust against slight change in the incoming frequencies although their strength can change. The peak at the level-spacing (cyclotron-energy) ω_c is the plasmon equiv-

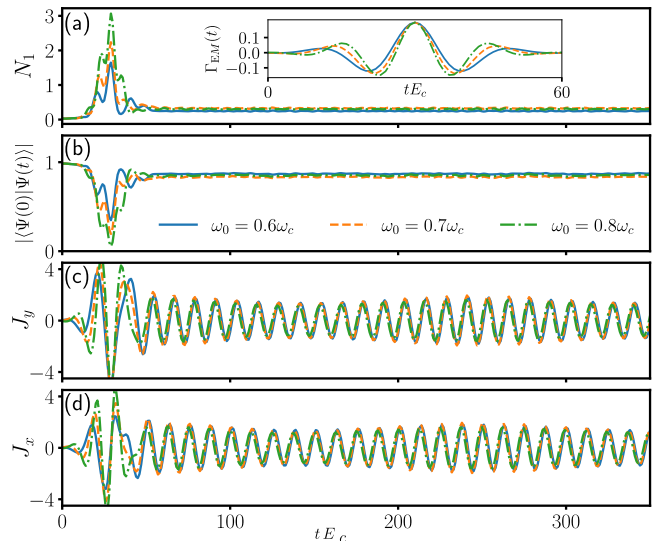


FIG. 3. Color online. Dynamical observables for various laser frequencies ω_0 (a) Number of excited electrons for various in-coming light frequencies in-set of (a) gives the form of $\Gamma_{EM}(t)$ (b) Fidelity $|\langle \Psi(0) | \Psi(t) \rangle|$. (c) The y-component of current from Eq. (5). d) x-component of the current. The quantities are obtained for $N = 6$ on torus with $L_2 = 10.63\ell_B$. The intensity is set to $eA_0/\sqrt{2}m^*\ell_B = 0.2E_c$ and $t_d = 10/E_c$. The units of time is the inverse of E_c . The usual values of E_c is around 14 meV [18] which gives 47 femto-seconds as the unit of time.

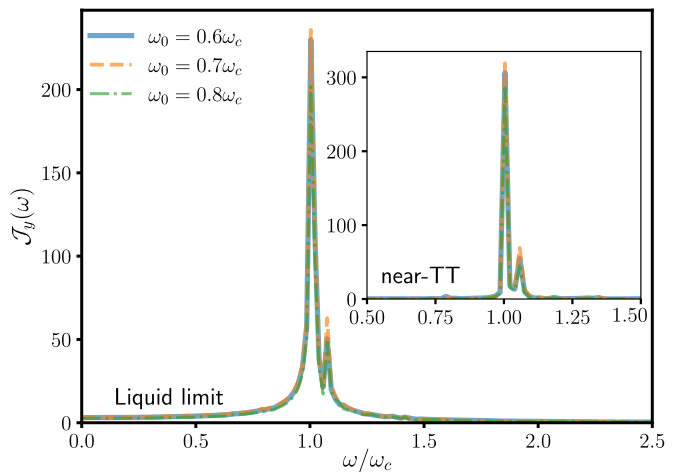


FIG. 4. Spectrum of $d[\hat{J}_y(t)]/dt$ following the pulse with parameters $eA_0/\sqrt{2}m^*\ell_B = 0.2E_c$ and $t_d = 10/E_c$. The incoming laser frequency is swept from $\omega_0 = 0.6 - 0.8\omega_c$. The behaviour of the current shows the excitation of a mode in addition to magnetoplasmon at frequency ω_c that is blue-shifted from ω_c . The system size is set to $N = 6$ and $L_y = \sqrt{2\pi}18\ell_B$. Inset gives the spectrum for near-TT limit ($L_y = 2\pi\ell_B$).

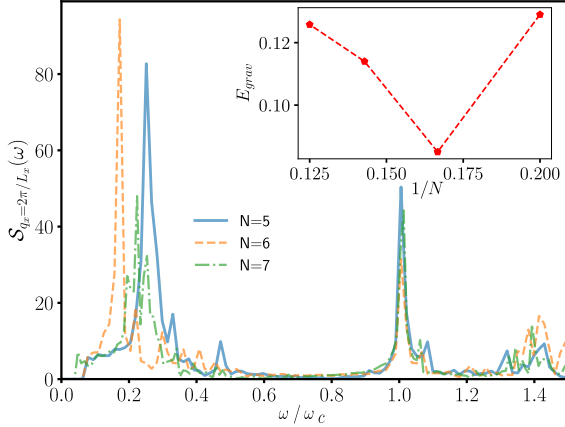


FIG. 5. Color online. Structure factor $\mathcal{S}(q_x = 2\pi/L_x, \omega)$ for different system sizes. The torus dimensions is taken $L_x = L_y = \sqrt{6\pi N}\ell_B$. The laser-frequency is $\omega_0 = 0.7\omega_c$ and other laser parameters are set as in Fig. 3.

alent of FQH state identified as $q \rightarrow 0$ limit of *magnetoplasmon* mode. This mode is due to single particle excitations from LLL to LL1 [18]. In the experiments, another peak that is blue shifted from magnetoplasmon has also been observed [18]. This mode was sometimes attributed to $q = 0$ spin-flip inter-Landau-level excitation involving enhanced exchange in spin-polarized state. We find blue-shifted peaks in our calculations are due to excitations of additional electron to LL1 although complete understanding is missing due to the presence of finite-size effects and the truncation to LL1.

The spectrum of structure factor $\mathcal{S}(\mathbf{q}, \omega)$ is shown in Fig. 5. It shows the existence of low-energy modes for different system sizes. The peak at $\omega/\omega_c = 1$ is magnetoplasmon mode discussed in the laser-field induced current spectrum. Significantly, there emerge new modes located at the energy around $0.2\omega_c$. We have also verified that in the low intensity regime of the laser pulse field, the magnetoplasmon mode and the new mode follow the linear and quadratic dependence of the field strength, respectively. To determine the nature of these new low-energy modes in $\mathcal{S}_{\mathbf{q}}(\omega)$, we evaluate the overlap $|\langle \Psi(t)|n\rangle|$ to analyze the weight of low-lying eigen-states $|n\rangle$ contained in the photo-induced excited state $|\Psi(t)\rangle$. The results are given in Table I. We have found that low-energy excitations are dominated by quadrupole FQH graviton states. These states are identified by matrix-element $I_n = |\langle \Psi_0|\hat{O}^{(2)}|n\rangle|$, where $\hat{O}^{(2)}$ is the operator with quadrupole structure and $|\Psi_0\rangle$ is our initial ground state before the application of laser pulse. The specific

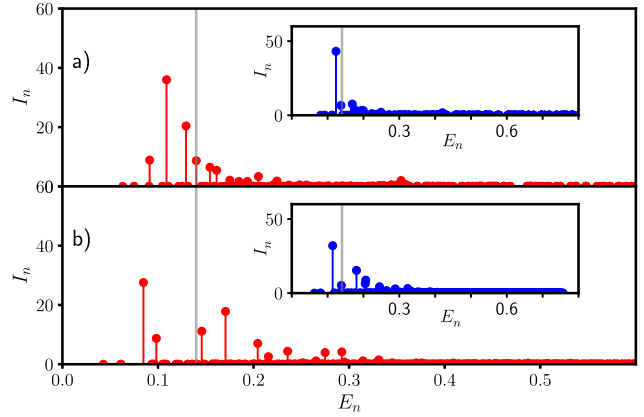


FIG. 6. Color online. (a) $I_n = |\langle \Psi_0|\hat{O}^{(2)}|n\rangle|$ for near-TT limit $L_y = 2\pi\ell_B$. Where $|\Psi_0\rangle$ is the FQH-1/3 state and $|n\rangle$ is the n -th excited state of Hamiltonian in Eq. (3). The inset of (a) gives the transition matrix element between FQH-1/3 state and the eigen-states of LLL. (b) Same as (a) but for quantum-liquid limit ($L_y = 10.63\ell_B$) for square torus. The inset of (b) gives the matrix element for the liquid-limit in LLL. The system size is $N = 6$ particles and the level-spacing is set to $0.5E_c$. Grey vertical line on plots is at energy $0.15E_c$.

form of $\hat{O}^{(2)}$ is given as [19]

$$\hat{O}^{(2)} = \sum_{\{j_i\}} \delta'_{j_1+j_2, j_3+j_4} \hat{O}_{qd}^{j_1, j_2, j_3, j_4} c_{0, j_1}^\dagger c_{0, j_2}^\dagger c_{0, j_3} c_{0, j_4} \quad (6)$$

$$\hat{O}_{qd}^{\{j_i\}} = \sum_{q=(s\frac{2\pi}{L_x}, t\frac{2\pi}{L_y})} \delta'_{j_1-j_4, t} \left(q_x^2 - q_y^2 \right) \frac{2\pi}{q} e^{-\frac{q^2}{2}} e^{-i2\pi s \frac{j_1-j_3}{N_\phi}}$$

In Fig. 6, we present the values of transition matrix element $\langle n|\hat{O}^{(2)}|\Psi_0\rangle$ (un-normalized) between FQH 1/3 state and $|n\rangle$ is the n -th excited state for two cases i) When $|n\rangle$ is the eigen-state of the system Hamiltonian involving all scattering processes and ii) when $|n\rangle$ is the eigen-state of LLL Hamiltonian where all scattering processes are confined to LLL. This transition matrix element represents the system transition rate due to an oscillating metric tensor analogous to the passing of a gravitation wave and hence usually termed as *graviton* [36]. This graviton mode occurs for both near-TT and liquid limit as shown in Fig. 6 (a) and (b). It is robust against the system size (See SM [34] for details). Moreover, as seen from Fig. 6, the energy of graviton states E_{grav} , when virtual processes are included, is slightly lower than the graviton states of a system when all interaction processes are confined to LLL. Furthermore, we follow Ref. 19 to analyze the handedness of this graviton and find it has the structure of $(q_x - iq_y)^2$, suggesting its chiral nature (See SM [34] for the detail of analysis.). Previously, it has also been proposed [37, 38] that graviton can be excited via geometric quench [39]. A variant of such graviton mode called chiral graviton mode has been observed in experiments recently for fractional Hall states

TABLE I. The contribution of states in $|\Psi(t)\rangle$ after the pulse for $N = 5$ and $N = 6$. ΔE denotes the energy difference from the ground state. Overlap $|\langle n|\Psi(t)\rangle|$ gives the contribution of individual eigen-state $|n\rangle$ of the system Hamiltonian with energy E_n . $\omega_c = 0.5E_c$.

Size ^a	$E_n (E_c)$	Overlap	$\Delta E (E_c)$	Nature ^b
$N = 6$	-1.38	0.84	0.0	G.S.
-	-1.296	0.092	0.084	Quadrupole
-	-1.2828	0.05	0.097	Quadrupole
-	-0.876	0.4288	ω_c	Plasmon
$N=5$	-1.067	0.882	0.0	G.S.
-	-0.9377	0.0934	0.129	Quadrupole
-	-0.562	0.396	$0.504 \approx \omega_c$	Plasmon
-	-0.091	0.086	0.543	Blue-shifted

^a The parameters of laser is set to $(eA_0/\sqrt{2}m^*\ell_B, \omega_0) = (0.2E_c, 0.7\omega_c)$ with $t_d = 10E_c$ and $L_y = \sqrt{2\pi N_\phi}\ell_B$. Similar results have been found for $N = 7$ and are also observed for near-TT limit.

^b Due to large Hilbert space size, we do not have eigen-state corresponding to Blue-shifted peak for $N = 6$. Similarly, for $N = 7$ we only have low-energy quadrupole states.

at filling fractional $\frac{1}{3}$ and $\frac{2}{5}$ fillings [20]. Chiral graviton modes in FQH system has been previously excited by tuning the laser-frequency near resonance conditions between valence and conduction band in 2D quantum wells. Our work has demonstrated that chiral graviton modes can also be excited when the a short-time laser is tuned near Landau level gap which is easily accessible experimentally. Furthermore, the excitation of graviton mode can be observed along with magneto-plasmon mode when all scattering processes are considered. We suggest to use a circularly polarized probe light to experimentally detect the chirality of the graviton mode.

Conclusions.— Through exact-diagonalization, the laser-induced dynamics of FQH state at $\nu = 1/3$ has been presented. We showed that laser-induced excitations of FQH states have rich physics. On the one hand, some excitations are coupled to electromagnetic field and can cause emission like the plasmon mode. On the other hand, we have shown that when scattering from LLL to LL1 is included in interactions, it is possible to excite neutral-modes of LLL through linearly polarized laser pulse field. These excitations are analogous to emergent *gravitons* due to their quadrupole structure and is the excitation of intrinsic metric carried by Hall fluids. Future experiments are needed to reveal how gap structure for fractional Hall systems evolve with finite momentum. Such experiments will not only address the questions related to strongly-interacting electron systems, but can also shed light on the understanding of the analogues of fundamental particles in high energy physics realized in condensed matter systems.

Acknowledgements.— A.K. thanks Avadh Saxena and Pouyan Ghaemi for their fruitful discussions. This work was carried out under the auspices of the U.S.

Department of Energy (DOE) National Nuclear Security Administration (NNSA) under Contract No. 89233218CNA000001. It was supported by LANL LDRD Program and Quantum Science Center, a U.S. DOE Office of Science Quantum Information Science Research Center. It was supported in part by Center for Integrated nanotechnologies, a DOE BES user facility, in partnership with the LANL Institutional Computing Program for computational resources.

* akirmani@lanl.gov

† benedikt.fauseweh@tu-dortmund.de

‡ jxzh@lanl.gov

- [1] F. D. M. Haldane, *Phys. Rev. Lett.* **107**, 116801 (2011).
- [2] D. Arovas, J. R. Schrieffer, and F. Wilczek, *Phys. Rev. Lett.* **53**, 722 (1984).
- [3] S. M. Girvin, A. H. MacDonald, and P. M. Platzman, *Phys. Rev. B* **33**, 2481 (1986).
- [4] S. M. Girvin, A. H. MacDonald, and P. M. Platzman, *Phys. Rev. Lett.* **54**, 581 (1985).
- [5] F. D. M. Haldane, “Hall viscosity and intrinsic metric of incompressible fractional hall fluids,” (2009), [arXiv:0906.1854 \[cond-mat.str-el\]](https://arxiv.org/abs/0906.1854).
- [6] S. Pu, M. Fremling, and J. K. Jain, *Phys. Rev. Res.* **2**, 013139 (2020).
- [7] N. Read and E. H. Rezayi, *Phys. Rev. B* **84**, 085316 (2011).
- [8] D. C. Tsui, H. L. Stormer, and A. C. Gossard, *Phys. Rev. Lett.* **48**, 1559 (1982).
- [9] H. L. Stormer, A. Chang, D. C. Tsui, J. C. M. Hwang, A. C. Gossard, and W. Wiegmann, *Phys. Rev. Lett.* **50**, 1953 (1983).
- [10] R. B. Laughlin, *Phys. Rev. Lett.* **50**, 1395 (1983).
- [11] F. D. M. Haldane, *Phys. Rev. Lett.* **51**, 605 (1983).
- [12] J. Nakamura, S. Liang, G. C. Gardner, and M. J. Manfra, *Nat. Phys.* **16**, 931 (2020).
- [13] P. Glidic, O. Maillet, C. Piquard, A. Aassime, A. Cavanaugh, Y. Jin, U. Gennser, A. Anthore, and F. Pierre, *Nat. Commun.* **14**, 514 (2023).
- [14] D. Yoshioka, B. I. Halperin, and P. A. Lee, *Phys. Rev. Lett.* **50**, 1219 (1983).
- [15] E. H. Rezayi and F. D. M. Haldane, *Phys. Rev. B* **50**, 17199 (1994).
- [16] M. Nakamura, Z.-Y. Wang, and E. J. Bergholtz, *Phys. Rev. Lett.* **109**, 016401 (2012).
- [17] P. Soulé and T. Jolicœur, *Phys. Rev. B* **85**, 155116 (2012).
- [18] A. Pinczuk, B. S. Dennis, L. N. Pfeiffer, and K. West, *Phys. Rev. Lett.* **70**, 3983 (1993).
- [19] S.-F. Liou, F. D. M. Haldane, K. Yang, and E. H. Rezayi, *Phys. Rev. Lett.* **123**, 146801 (2019).
- [20] J. Liang, Z. Liu, Z. Yang, Y. Huang, U. Wurstbauer, C. R. Dean, K. W. West, L. N. Pfeiffer, L. Du, and A. Pinczuk, *Nature* **628**, 78 (2024).
- [21] A. Ghazaryan, T. Graß, M. J. Gullans, P. Ghaemi, and M. Hafezi, *Phys. Rev. Lett.* **119**, 247403 (2017).
- [22] Z.-P. Cian, T. Grass, A. Vaezi, Z. Liu, and M. Hafezi, *Phys. Rev. B* **102**, 085430 (2020).
- [23] B. I. Halperin, *Helv. Phys. Acta* **56**, 75 (1983).

- [24] S. He, S. Das Sarma, and X. C. Xie, *Phys. Rev. B* **47**, 4394 (1993).
- [25] J. P. Eisenstein, G. S. Boebinger, L. N. Pfeiffer, K. W. West, and S. He, *Phys. Rev. Lett.* **68**, 1383 (1992).
- [26] Y. W. Suen, L. W. Engel, M. B. Santos, M. Shayegan, and D. C. Tsui, *Phys. Rev. Lett.* **68**, 1379 (1992).
- [27] N. C. Bishop, M. Padmanabhan, K. Vakili, Y. P. Shkolnikov, E. P. De Poortere, and M. Shayegan, *Phys. Rev. Lett.* **98**, 266404 (2007).
- [28] M. Padmanabhan, T. Gokmen, and M. Shayegan, *Phys. Rev. B* **80**, 035423 (2009).
- [29] B. Yang, Z. Papić, E. H. Rezayi, R. N. Bhatt, and F. D. M. Haldane, *Phys. Rev. B* **85**, 165318 (2012).
- [30] B. Fauseweh and J.-X. Zhu, *Phys. Rev. B* **102**, 165128 (2020).
- [31] A. Seidel, H. Fu, D.-H. Lee, J. M. Leinaas, and J. Moore, *Phys. Rev. Lett.* **95**, 266405 (2005).
- [32] S. A. Trugman and S. Kivelson, *Phys. Rev. B* **31**, 5280 (1985).
- [33] Z. Papić and A. C. Balram, “Fractional quantum hall effect in semiconductor systems,” (2022), [arXiv:2205.03421](https://arxiv.org/abs/2205.03421) [[cond-mat.mes-hall](https://arxiv.org/abs/2205.03421)].
- [34] Supplemental Material for Laser-driven Ultrafast Dynamics of a Fractional Quantum Hall System.
- [35] I. Sodemann and A. H. MacDonald, *Phys. Rev. B* **87**, 245425 (2013).
- [36] K. Yang, *Phys. Rev. B* **93**, 161302 (2016).
- [37] A. Kirmani, K. Bull, C.-Y. Hou, V. Saravanan, S. M. Saeed, Z. Papić, A. Rahmani, and P. Ghaemi, *Phys. Rev. Lett.* **129**, 056801 (2022).
- [38] Z. Liu, A. Gromov, and Z. Papić, *Phys. Rev. B* **98**, 155140 (2018).
- [39] Z. Liu, A. C. Balram, Z. Papić, and A. Gromov, *Phys. Rev. Lett.* **126**, 076604 (2021).

Supplementary Material.

February 10, 2025

1 Hamiltonian

We truncate our model to the first Landau level and define $q = q_x - iq_y$

$$\begin{aligned} C_{n_1, n_4}(\mathbf{q}) &= \sqrt{\frac{n_4!}{n_1!}} \left(\frac{iq\ell_B}{\sqrt{2}} \right)^{n_1 - n_4} L_{n_4 - n_1}^{n_4 - n_1} \left(\frac{(q_x^2 + q_y^2)\ell_B^2}{2} \right), \quad n_1 \geq n_4 \\ C_{n_1, n_4}(\mathbf{q}) &= \sqrt{\frac{n_1!}{n_4!}} \left(\frac{iq^*\ell_B}{\sqrt{2}} \right)^{n_1 - n_4} L_{n_4 - n_1}^{n_1 - n_4} \left(\frac{(q_x^2 + q_y^2)\ell_B^2}{2} \right), \quad n_1 \leq n_4 \end{aligned} \quad (1)$$

$$V_{j_1, j_2, j_3, j_4}^{n_1, n_2, n_3, n_4} = \delta'_{j_1 + j_2, j_3 + j_4} \frac{1}{2L_1 L_2} \sum_{\mathbf{q} = \left(s \frac{2\pi}{L_1}, t \frac{2\pi}{L_2} \right)} \delta'_{j_1 - j_4, t} V(\mathbf{q}) C_{n_1, n_4}(-q_x, -q_y) C_{n_2, n_3}(q_x, q_y) e^{-i2\pi s(j_1 - j_3)/N_\phi} e^{-\frac{q^2}{2}\ell_B^2} \quad (2)$$

Where δ' is defined modulo N_ϕ and \mathbf{q}' represents that $\mathbf{q} = 0$ is eliminated. $V(\mathbf{q}) = \frac{2\pi}{\varepsilon q}$ for Coulomb and $V(\mathbf{q}) = -q^2$ for Haldane pseudo-potential.

1.1 Projected density operators and structure factor

Let us consider the single-particle orbitals for torus boundary conditions

$$\phi_{n,j}(\mathbf{r}) = \frac{1}{\sqrt{N_n}} \sum_l e^{iyX_{j,l}} e^{-\frac{(x+X_{j,l})^2}{2}} H_n \left(\frac{x + X_{j,l}}{\ell_B} \right) \quad (3)$$

Where $X_{j,l} = \frac{2\pi\ell_B^2}{L_y} j + lL_x$. We set $\ell_B = 1$ and define $\kappa = \frac{2\pi}{L_y}$

$$\begin{aligned} I_{j,k}^{n,n'}(\mathbf{q}) &= \frac{1}{\sqrt{N_n N_{n'}}} \int d\mathbf{r} e^{i\mathbf{q}\cdot\mathbf{r}} \phi_{n,j}^*(\mathbf{r}) \phi_{n',k}(\mathbf{r}) \\ I_{j,k}^{0,0}(\mathbf{q}) &= \sum_{\Delta} \delta_{\frac{q_y}{\kappa}, (j-k) + \Delta N_\phi} e^{-\frac{q^2}{4}} e^{-i\frac{q_x}{2}(X_j + X_k + \Delta L_x)} \\ I_{j,k}^{1,0}(\mathbf{q}) &= \frac{1}{\sqrt{2}} \sum_{\Delta} \delta_{\frac{q_y}{\kappa}, (j-k) + \Delta N_\phi} \left(q_y + iq_x \right) e^{-\frac{q^2}{4}} e^{-i\frac{q_x}{2}(X_j + X_k + \Delta L_x)} \\ I_{j,k}^{0,1}(\mathbf{q}) &= \frac{1}{\sqrt{2}} \sum_{\Delta} \delta_{\frac{q_y}{\kappa}, (j-k) + \Delta N_\phi} \left(-q_y + iq_x \right) e^{-\frac{q^2}{4}} e^{-i\frac{q_x}{2}(X_j + X_k + \Delta L_x)} \\ I_{j,k}^{1,1}(\mathbf{q}) &= \frac{1}{2} \sum_{\Delta} \delta_{\frac{q_y}{\kappa}, (j-k) + \Delta N_\phi} \left(2 - \mathbf{q}^2 \right) e^{-\frac{q^2}{4}} e^{-i\frac{q_x}{2}(X_j + X_k + \Delta L_x)} \end{aligned} \quad (4)$$

$$\begin{aligned}
\hat{\rho}_{\mathbf{q}}^{0,0} &= \sum_{\Delta,j,k} \delta_{\frac{q_y}{\kappa},(j-k)+\Delta N_\phi} e^{-\frac{q^2}{4}} e^{-i\frac{q_x}{2}(X_j+X_k+\Delta L_x)} c_{0,j}^\dagger c_{0,k} \\
\hat{\rho}_{\mathbf{q}}^{1,0} &= \frac{1}{\sqrt{2}} \sum_{\Delta,j,k} \delta_{\frac{q_y}{\kappa},(j-k)+\Delta N_\phi} \left(q_y + iq_x \right) e^{-\frac{q^2}{4}} e^{-i\frac{q_x}{2}(X_j+X_k+\Delta L_x)} c_{1,j}^\dagger c_{0,k} \\
\hat{\rho}_{\mathbf{q}}^{0,1} &= \frac{1}{\sqrt{2}} \sum_{\Delta,j,k} \delta_{\frac{q_y}{\kappa},(j-k)+\Delta N_\phi} \left(-q_y + iq_x \right) e^{-\frac{q^2}{4}} e^{-i\frac{q_x}{2}(X_j+X_k+\Delta L_x)} c_{0,j}^\dagger c_{1,k} \\
\hat{\rho}_{\mathbf{q}}^{1,1} &= \frac{1}{2} \sum_{\Delta,j,k} \delta_{\frac{q_y}{\kappa},(j-k)+\Delta N_\phi} \left(2 - \mathbf{q}^2 \right) e^{-\frac{q^2}{4}} e^{-i\frac{q_x}{2}(X_j+X_k+\Delta L_x)} c_{1,j}^\dagger c_{1,k}
\end{aligned} \tag{5}$$

Given the above relations in Eq. (5),

$$\hat{\rho}_{\mathbf{q}} = \hat{\rho}_{\mathbf{q}}^{0,0} + \hat{\rho}_{\mathbf{q}}^{1,0} + \hat{\rho}_{\mathbf{q}}^{0,1} + \rho_{\mathbf{q}}^{1,1} \tag{6}$$

The structure factor is then given by,

$$\mathcal{S}_{\mathbf{q}} = \hat{\rho}_{\mathbf{q}} \hat{\rho}_{-\mathbf{q}} \tag{7}$$

It is not difficult to get $\rho_{-\mathbf{q}}$ by inverting the momentum for example inverting momentum in $\rho_{\mathbf{q}}^{0,0}$ gives $\hat{\rho}_{-\mathbf{q}}^{0,0} = \sum_{\Delta,j,k} \delta_{-\frac{q_y}{\kappa},(j-k)+\Delta N_\phi} e^{-\frac{q^2}{4}} e^{+i\frac{q_x}{2}(X_j+X_k+\Delta L_x)} c_{0,j}^\dagger c_{0,k}$.

2 Low energy quadrupole excitations and handedness

We follow [?] in this section.

$$\hat{O}^{(2)} = \sum_{\{j_i\}} \sum'_{q=(s\frac{2\pi}{L_x}, t\frac{2\pi}{L_y})} \delta'_{j_1+j_2,j_3+j_4} \delta'_{j_1-j_4,t} \left(q_x^2 - q_y^2 \right) V_{\mathbf{q}} e^{-\frac{q^2}{2}} e^{-i2\pi s\frac{j_1-j_3}{N_\phi}} c_{0,j_1}^\dagger c_{0,j_2}^\dagger c_{0,j_3} c_{0,j_4} \tag{8}$$

Where prime over summation means that $q = 0$ is excluded and prime over delta functions means that they are defined modulo N_ϕ . The chiral variant of Eq. (8) [?].

$$\hat{O}_{\mp}^{(2)} = \sum_{\{j_i\}} \sum'_{q=(s\frac{2\pi}{L_x}, t\frac{2\pi}{L_y})} \delta'_{j_1+j_2,j_3+j_4} \delta'_{j_1-j_4,t} \left(q_x \mp iq_y \right)^2 \frac{2\pi}{q} e^{-\frac{q^2}{2}} e^{-i2\pi s\frac{j_1-j_3}{N_\phi}} c_{0,j_1}^\dagger c_{0,j_2}^\dagger c_{0,j_3} c_{0,j_4} \tag{9}$$

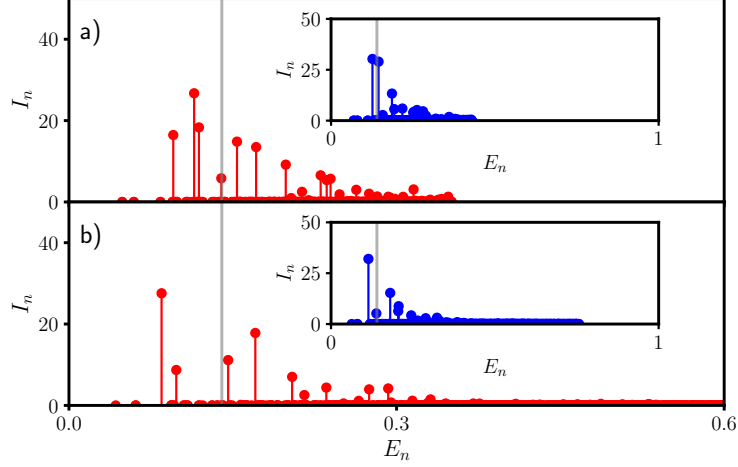


Figure 1: Color online. (a) $I_n = |\langle \Psi_0 | \hat{O}^{(2)} | n \rangle|$ for $N = 7$ for $L_y = \sqrt{2\pi 21} \ell_B$. Where $|\Psi_0\rangle$ is the FQH-1/3 state and $|n\rangle$ is the n -th excited state of Hamiltonian. The inset of (a) gives the transition matrix element between FQH-1/3 state and the eigen-states of LLL. (b) Same as (a) but for $N = 6$ and $L_y = \sqrt{2\pi 18} \ell_B$. The level-spacing is set to $0.5E_c$. Grey vertical line on plots is at energy $0.15E_c$.

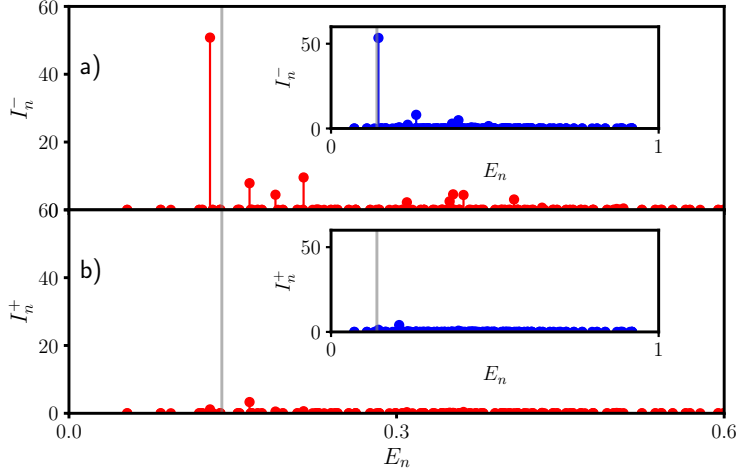


Figure 2: Color online. (a) $I_n^- = |\langle \Psi_0 | \hat{O}_-^{(2)} | n \rangle|$ for $N = 5$ and $L_y = \sqrt{2\pi 15} \ell_B$. Where $|\Psi_0\rangle$ is the FQH-1/3 state and $|n\rangle$ is the n -th excited state of Hamiltonian with all inter- and intra-level interaction. The inset of (a) gives the transition matrix element between FQH-1/3 state and the eigen-states of LLL. (b) $I_n^+ = |\langle \Psi_0 | \hat{O}_+^{(2)} | n \rangle|$ showing suppression with all parameters same as (a). The level-spacing is set to $0.5E_c$. $V_{\mathbf{q}} = \frac{2\pi}{\varepsilon q}$ is used.

From figure 1 and 2, we can conclude that our state our graviton excitations are also chiral as reference [?].

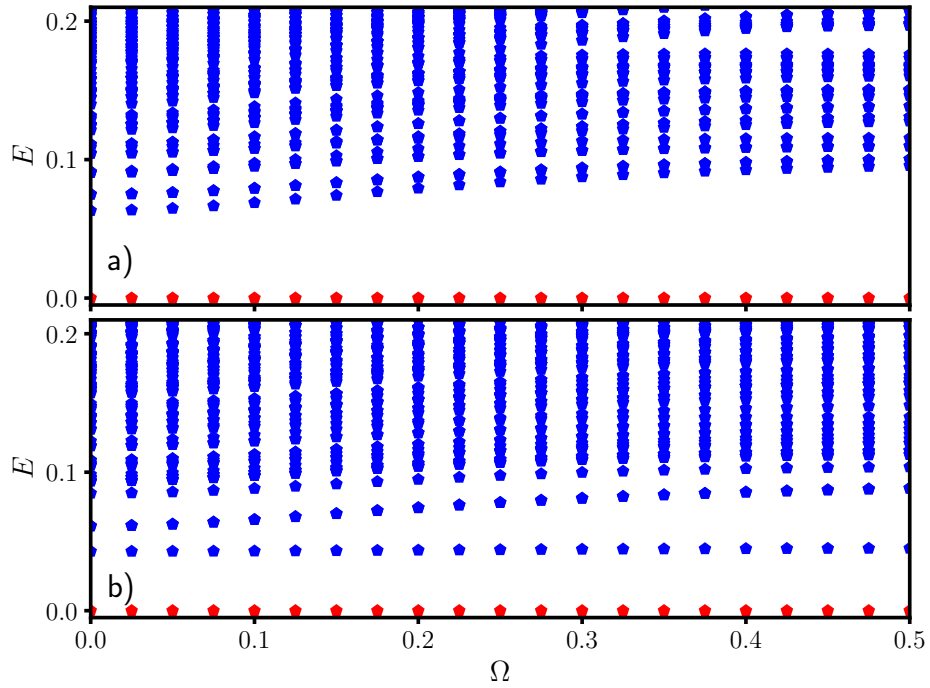


Figure 3: Color online. Low energy spectrum of Eq. (2) at $\nu = 1/3$ for $\delta = 0.5E_c$ at various values of Ω . (a) The circumference of the torus is set $b = 2\pi\ell_B$ for near thin torus limit. (b) The circumference of the torus is set $b = \sqrt{2\pi 18}\ell_B$ for the liquid limit. The particle number is set to 6. The ground-state energy is shifted to 0 (red pentagons).

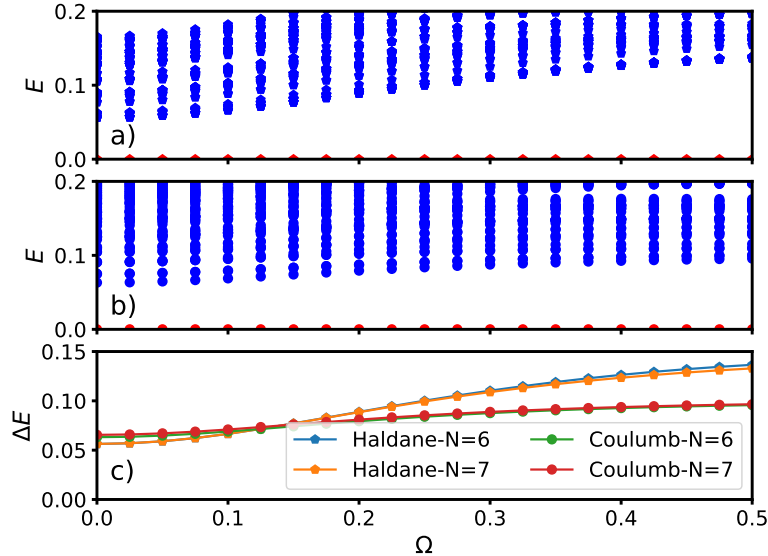


Figure 4: a) The low-energy spectrum of Haldane pseudo-potential Hamiltonian on torus for $N=6$ electrons at $1/3$ filling. b) Same as (a) but for Coulomb's potential. c) The energy gap to the excited state for different interactions and for various system sizes. The circumference of the torus is set to $L_y = 2\pi\ell_B$.

3 Low Energy Physics

The equilibrium physics of Hamiltonian in Eq. (2) can be explained by replacing $A_{EM}(t)$ by a static-field Ω that controls the amount of hopping between LLL and LL1. Fig. 3 shows the low-energy spectrum of Hamiltonian of Eq. (2) at $1/3$ filling against various values of Ω . The gap of ground state (G.S.) to the first excited state is robust for both near-TT limit (Fig. 3-a) and the liquid-limit 3-b). As Ω is increased, the excited state remains gapped from the ground state, although it is unclear how the G.S. for non-zero Ω is related to FQH $1/3$ state.

To understand the low energy physics of our two-level model and its dynamics, we first establish the effect of inter-level two-body scattering for finite level spacing in the absence of the pulse field. For V_1 ($V_q \propto -q^2$) Haldane-pseudopotential the presence of inter-level scattering process do not affect the fractional $1/3$ Hall ground state. We evaluate the overlap of the ground state of our model with inter-level scattering processes with fractional Hall $1/3$ state. We have found that fractional Hall $1/3$ state for Haldane-pseudopotential is the ground state of our model even for small ω_c . Thus we can use our initial fractional $1/3$ Hall state to be the ground state of our system. For Coulomb potential on torus, the situation is similar but only at finite level-spacing ω_c , the overlap with the fractional Hall $1/3$ state recovers as shown in figure 5 of Appendix.

We also plot the energy gap between the ground state and the first excited state on cylinder and torus for V_1 interactions in Fig. 4. We see that for different system sizes, the system is gapped for all values of Ω_0 . The same hold true for Coulomb interactions on torus.

4 Spectral Function

We are interested in spectral function $\langle \Psi(t_i) | \{ \hat{c}_{k,l}^\dagger(t_f), \hat{c}_{k,l}(t_i) \} | \Psi(t_i) \rangle$. First consider $|\Psi(t_i)\rangle = \sum_n c_n |n\rangle$ where $c_n = \langle n | \Psi(t_i) \rangle$

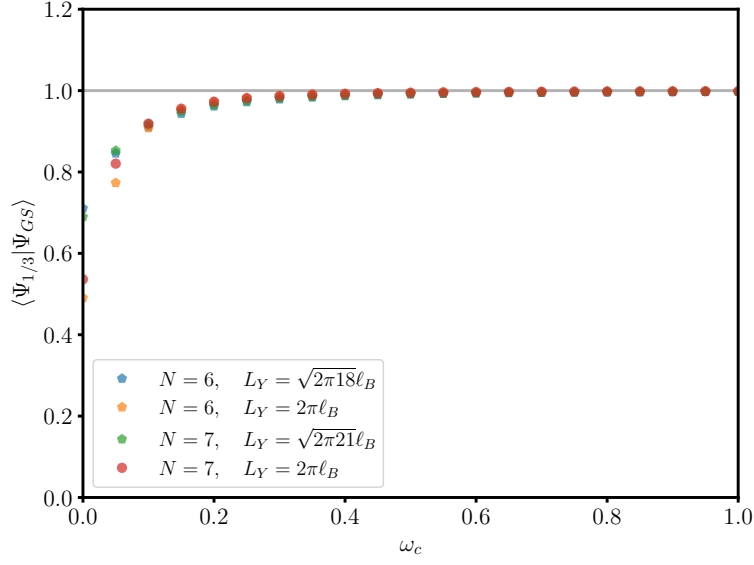


Figure 5: The overlap of fractional 1/3 state in LLL with the ground state of Hamiltonian for Coulomb interactions on torus. The Hamiltonian has all matrix elements including Landau-level non-conserving interactions. ω_c is in the units of $e^2/\varepsilon\ell_B$.

$$A_{k,l,l'}^1(t) = \langle \Psi(t_i) | e^{iHt_f} \hat{c}_{k,l}^\dagger e^{-iHt_f} e^{iHt_i} \hat{c}_{k,l'}(t_i) e^{-iHt_i} | \Psi(t_i) \rangle \quad (10)$$

$$= \sum_{\bar{n}} \langle \Psi(t_i) | e^{iHt_f} \hat{c}_{k,l}^\dagger e^{-iHt_f} e^{iHt_i} | \bar{n} \rangle \langle \bar{n} | \hat{c}_{k,l'} e^{-iHt_i} | \Psi(t_i) \rangle \quad (11)$$

$$= \sum_{\bar{n}} e^{-iE_{\bar{n}}(t_f - t_i)} \langle \Psi(t_i) | e^{iHt_f} \hat{c}_{k,l}^\dagger | \bar{n} \rangle \langle \bar{n} | \hat{c}_{k,l'} e^{-iHt_i} | \Psi(t_i) \rangle \quad (12)$$

$$= \sum_{\bar{n}, m, n} e^{-iE_{\bar{n}}(t_f - t_i)} e^{iE_m t_f} e^{-iE_n t_i} c_m^* c_n \langle m | \hat{c}_{k,l}^\dagger | \bar{n} \rangle \langle \bar{n} | \hat{c}_{k,l'} | n \rangle \quad (13)$$

5 Current

The current is obtained by infinitesimally changing the gauge potential from $A = (0, Bx, 0)$ to A' in single-particle Hamiltonian and evaluating the difference $\hat{H}_{sp}(A') - \hat{H}_{sp}(A)$. Where $A' = A + \delta A_x \hat{x}$ for the x-component and $A' = A + \delta A_y \hat{y}$ for the y-component of the current respectively. The difference is then divided by δA_x and δA_y .

Although, there is no net current due to the conservation of particle number, there is still a local time-dependent distribution of current e.g. along x-axis representing density-oscillations.

6 Computations

In this section we will present more runs e.g. Fig. 5 shows the same behavior as the main text for sizes $N = 5, 6, 7$ for square torus.

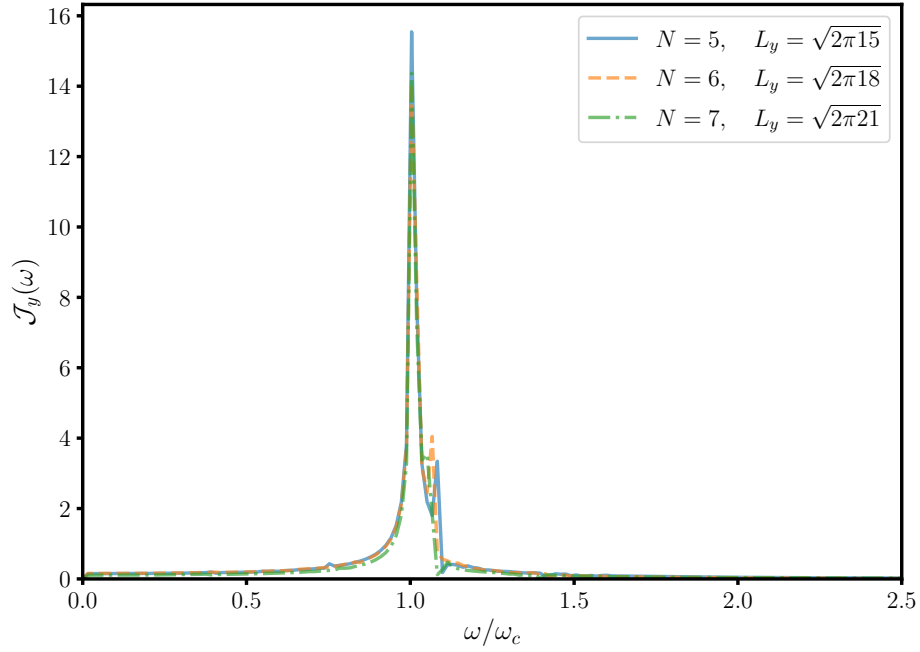


Figure 6: Different runs for square torus $L_y = L_x = \sqrt{2\pi N_\phi} \ell_B$. The laser parameters are set to $(eA_0/\sqrt{2}m^* \ell_B, \omega_0) = (0.2, 0.7\omega_c)$ and $\omega_c = 0.5E_c$.

Figure 7: Multiple system size runs for $\omega_c = 0.5E_c$.

7 Spectrum

Let us consider T be the time that laser-pulse is finished and the wave-function at time T is $\Psi(T) = \sum_n \bar{c}_n |n\rangle$. Since, the Hamiltonian is time-independent after the pulse is finished, $\Psi(t > T) = e^{-iH(t-T)} |\Psi(T)\rangle$

$$\begin{aligned}
\langle \hat{J}(t < T) \rangle &= \langle \Psi(t) | \hat{J} | \Psi(t) \rangle = \sum_{n,m} \langle n | \hat{J} | m \rangle \langle \Psi(t > T) | |n\rangle \langle m| | \Psi(t > T) \rangle \\
&= \sum_{n,m} \langle n | \hat{J} | m \rangle \langle \Psi(T) | e^{iH(t-T)} |n\rangle \langle m| e^{-iH(t-T)} | \Psi(T) \rangle \\
&= \sum_{n,m} \langle n | \hat{J} | m \rangle e^{iE_n(t-T)} \bar{c}_n^* \bar{c}_m e^{-iE_m(t-T)}
\end{aligned} \tag{14}$$

Taking Fourier transform

$$\begin{aligned}
\mathcal{F} \left[\frac{d\langle \hat{J}(t < T) \rangle}{dt} \right] (\omega) &= \sum_{n,m} i(E_n - E_m) \langle n | \hat{J} | m \rangle \bar{c}_n^* \bar{c}_m \int_T^\infty e^{i(E_n - E_m)(t-T)} e^{i\omega t} e^{-\eta t} dt \\
&= (E_n - E_m) \frac{-i}{(E_n - E_m + \omega + i\eta)}
\end{aligned} \tag{15}$$

Thus the modes appearing in the spectrum of the current are at frequencies $E_m - E_n$